Quantitative Measurement of Relaxation Interference Effects between ^1H_N CSA and $^1H-^{15}N$ Dipolar Interaction: Correlation with Secondary Structure

Marco Tessari, Hans Vis,† Rolf Boelens, Robert Kaptein, and Geerten W. Vuister*

Contribution from the Department of NMR Spectroscopy, Bijvoet Center for Biomolecular Research, Utrecht University, Padualaan 8, 3584 CH Utrecht, The Netherlands

Received February 24, 1997. Revised Manuscript Received May 1, 1997[⊗]

Abstract: An experiment is presented that allows the quantitative measurement of the cross-correlation rate between ^1H_N CSA and $^1H_N-^{15}N$ dipolar interaction in uniformly ^{15}N-enriched samples. The CSA/DD cross-correlation rate is obtained from the intensity ratio of an experiment in which the CSA/DD cross-correlation is active for a fixed time, τ, with a reference experiment in which it is inactive. The CSA/DD cross-correlation rates of 75 residues of the HU protein from *Bacillus stearothermophilus* were obtained from the linear fits of CSA/DD to reference ratios recorded for five values of τ and at two different B_o fields. After correction for the mobility of the $^1H-^{15}N$ bond vector the values of $(\sigma_{||} - \sigma_{\perp})(3\cos^2(\theta) - 1)/2$, containing information about the chemical shielding anisotropy, were derived for individual amide protons. The average value of 13 ± 5 ppm compares well with the results from previous solid state NMR measurements. The data also show a dependence upon hydrogen bonding and secondary structure: residues in α-helical conformation show values of 9 ± 4 ppm, whereas residues in β-sheet conformation show substantially higher values of 16 ± 6 ppm.

Introduction

Hydrogen bonds are of great importance in biological systems because of their role in secondary and tertiary structure formation and molecular recognition. The presence of these hydrogen bonds is usually inferred from a detailed analysis of biomolecular structures at atomic resolution, obtained from X-ray or high-resolution NMR studies, by searching for suitable donor and acceptor atoms in a proper hydrogen bonding conformation. Experimental evidence to support hydrogen bond formation provides valuable additional information. For example, amide protons which exchange slowly with the solvent are typically considered to be either involved in hydrogen bonds or have limited solvent accessibility.[1] Also solid-state ^1H NMR measurements can provide information on hydrogen bond formation. Measurements on small molecules have established a correlation between the strength of hydrogen bonding and isotropic chemical shift or chemical shift anisotropy (CSA) for hydroxyl protons involved in O−H···O bonds.[2,3]

Information about the CSA of protons would also be of great interest in biological systems. In principle, such information could be obtained from solid-state NMR experiments, but unfortunately several complications affect proton CSA measurements on biological macromolecules. Only a few experimental observations have so far been reported, limited to small synthetic peptides.[4−6] As a consequence, little is known about the dependence on secondary and tertiary structure of the value and orientation of chemical shift tensors for protons in macromolecules.

High-resolution solution NMR experiments provide a convenient method for measuring NMR parameters such as chemical shifts, NOEs, and T_1 and T_2 relaxation times at a large number of sites in a biological macromolecule, in particular if isotopic labeling is used to increase the resolution and sensitivity.[7,8] Relaxation interference effects between CSA and dipolar couplings contain information on motional properties and chemical shift tensors. For small molecules, these effects have been reported and analyzed in detail on several occasions.[9−15] Interference effects between ^1H_N CSA and dipolar interaction (DD) have also been observed in proteins and RNA before.[16,17] The differential relaxation rates observed for the doublet components of the imino protons in ^{15}N-substituted tRNA[18] were explained in terms of the CSA/DD cross-correlation mechanism. From the study on a model compound the CSA of the imino proton was calculated to be 5.7 ppm.[18] For proteins no quantitative analysis was performed thusfar. A DQF-NOESY

* Author to whom correspondence should be addressed.
† Current address: Oxford Center for Molecular Science, New Chemistry Laboratory, University of Oxford, South Parks Road, Oxford OX1 3QT, United Kingdom.
⊗ Abstract published in *Advance ACS Abstracts,* July 1, 1997.

(1) Wüthrich K. *NMR of Proteins and Nucleic Acids;* John Wiley & Sons: New York, 1986.
(2) Haeberlen, U. *High Resolution NMR in Solids: Selective Averaging*; Waugh, J. S. Ed.; Advances in Magnetic Resonance Supplement 1; Academic Press: New York 1976.
(3) Berglund, B.; Vaughan, R. W. *J. Chem. Phys.* **1980**, *73*, 2037−2043.
(4) Wu, C. H.; Ramamoorthy, A.; Gierasch, L. M., Opella, S. J. *J. Am. Chem. Soc.* **1995**, *117*, 6148−6149.
(5) Gerald, R., II; Bernhard, T.; Haeberlen, U.; Rendell, J.; Opella, S. *J. Am. Chem. Soc.* **1993**, *115*, 777−782.
(6) Ramamoorthy, A.; Gierasch, L. M.; Opella, S. J. *J. Magn. Reson. A* **1995**, *109*, 112−116.
(7) Clore, M. G.; Gronenborn, A. In *Methods in Enzymology*; James, T. L., Oppenheimer, N. J., Eds.; Academic Press: San Diego, 1994; Vol. 239, Part C, pp 349−363.
(8) Peng, J. W.; Wagner, G. In *Methods in Enzymology*; James, T. L., Oppenheimer, N. J., Eds.; Academic Press: San Diego, 1994; Vol. 239, Part C, pp 563−596.
(9) McConnell, H. M. J. *J. Chem. Phys.* **1956**, *25*, 709−711.
(10) Mackor, E. L.; MacLean, C. *Prog. Nucl. Magn. Reson. Spectrosc.* **1967**, *3*, 129−157.
(11) Goldman, M. *J. Magn. Reson.* **1984**, *60*, 437−452.
(12) Wimperis, S.; Bodenhausen, G. *Mol. Phys.* **1989**, *66*, 897−919.
(13) Bruschweiler, R.; Ernst, R. R. *J. Chem. Phys.* **1992**, *96*, 1758−1766.
(14) Burghardt, I.; Konrat, R.; Bodenhausen, G. *Mol. Phys.* **1992**, *75*, 467−486.
(15) Werbelow, L. G. in *Encyclopedia of Nuclear Magnetic Resonance*; Grant, D. M., Harris, R. K., Editors-in-Chief; Wiley: London, 1996; Vol. 6, pp 4072−4078.
(16) Dalvit, C. *J. Magn. Reson.* **1992**, *97*, 645−650.
(17) Ruterjans, H.; Kaun, E.; Hull, W. E.; Limbach, H. H. *Nucleic Acids Res.* **1982**, *10*, 7027−7039.
(18) Gueron, M.; Leroy, J. L.; Griffey, R. J. *J. Am. Chem. Soc.* **1983**, *105*, 7262−7266.

S0002-7863(97)00573-8 CCC: $14.00

experiment was proposed by Dalvit in order to observe the two-spin longitudinal order generated by ^1H_N CSA/DD($^1H_N-^1H_\alpha$) cross correlation in small molecules.[19] For ^{15}N-labeled proteins, Dalvit presented an HSQC-type experiment in which antiphase magnetization was generated by ^1H_N CSA/DD($^1H_N-^{15}N$) cross-correlation terms.[16] Recently, Tjandra et al.[20] have shown that the quantitative measurement of the cross-correlation between ^{15}N CSA and $^1H-^{15}N$ dipolar interaction in ^{15}N-labeled proteins can provide information on the magnitude of the ^{15}N chemical shift tensor.

Here, we present a pulse sequence for the quantitative measurement of the cross correlation between ^1H_N CSA and $^1H_N-^{15}N$ dipolar interaction in uniformly ^{15}N-enriched samples. The method is applied to the HU protein from *Bacillus stearothermophilus* (HUBst), a symmetric dimer of 19 kDa. The solution structure of HUBst was determined by high-resolution multidimensional heteronuclear NMR spectroscopy,[21,22] and its dynamic properties were studied recently by ^{15}N relaxation studies at multiple fields.[23] After correction for the dynamic properties of the backbone amides, the data yield information on the anisotropy of the ^1H_N chemical shift tensor for 75 residues in HUBst. The magnitude of the ^1H_N chemical shift tensor shows a dependence upon hydrogen bond formation. Moreover, a clear distinction between residues in α-helical and β-sheet conformation is observed, providing the first insight into the dependence of the anisotropy of the ^1H_N chemical shift tensor on secondary structure in a biological macromolecule.

Experimental Section

All NMR experiments were performed at 311 K on a 1.0 mM solution of uniformly ^{15}N labeled HUBst protein in 90% ^1H_2O/10% ^2H_2O, in the presence of 30 mM KP_i buffer at pH 4.6 and 100 mM KCl. Two data sets were acquired at 499.91 and 750.11 MHz ^{1}H resonance frequency with Varian UNITYplus 500 and UNITYplus 750 spectrometers, both equipped with a triple-resonance HCN probe with a shielded *z*-gradient coil. Each dataset consisted of five 2D experiments acquired with scheme A at different duration of the period Δ and a reference experiment acquired with scheme B (cf. Figure 1). 2D data matrices acquired at 500 and 750 MHz consisted of $160(t_1) \times 512(t_2)$ and $128(t_1) \times 512(t_2)$ complex points, respectively. For both the buildup series (scheme A) and the reference experiment (scheme B), an identical number of scans were collected (128 at 750 MHz and 64 at 500 MHz).

All data sets were processed with NMRPipe,[24] using 72° shifted squared sine-bell apodization in both dimensions, prior to zero filling to $1024(t_1) \times 2048(t_2)$ complex points, and Fourier transformation. The peaks were fitted to Gaussian profiles in both the F_1 and F_2 dimensions by using one of the NMRPipe software tools,[24] nlinLS for nonlinear least-squares minimization. The fit with five adjustable parameters (F_2 position, F_2 width, F_1 position, F_1 width, and amplitude) accounted for more than 95% of the observed intensity.

The one-parameter linear fit of the intensities of the peaks in the buildup series recorded with scheme A was performed by using an in-house implementation in OCTAVE of a linear least-squares routine.

Theory

Although dipolar proton−proton interactions provide a non-negligible relaxation mechanism for the amide protons, the simplifying assumption of an isolated $^{15}N-^1H_N$ spin pair will be considered first. The results for a more general system including dipolar interactions between the $^{15}N-^1H_N$ pair and other protons will be presented in the Results and Discussion section.

A detailed description of the interference effects on the relaxation of two unlike spins $^1/_2$ was presented by Goldman,[11] and therefore his treatment will be only briefly summarized. In the following, proton and nitrogen angular momentum operators will be indicated with **I** and **S**, respectively.

In the presence of cross terms between CSA(^1H_N) and DD($^1H_N-^{15}N$), the two components of the proton doublet relax at a different rate. For $^1J_{NH_N} < 0$, the transverse relaxation rates R_2^α and R_2^β of the low-field and high-field component, respectively, are[11]

$$R_2^\alpha = \lambda + \eta \tag{1a}$$

$$R_2^\beta = \lambda - \eta \tag{1b}$$

where λ is the autorelaxation rate and η is the cross-correlation relaxation rate. After a relaxation period of duration τ, the two components of the proton transverse magnetization are

$$\mathbf{I}_+^\alpha = \mathbf{I}_+^\alpha(0)\,\exp[-(\lambda+\eta)\tau] = \mathbf{I}_+^\alpha(0)\,\mathrm{E}(+,\tau) \tag{2a}$$

$$\mathbf{I}_+^\beta = \mathbf{I}_+^\beta(0)\,\exp[-(\lambda-\eta)\tau] = \mathbf{I}_+^\beta(0)\,\mathrm{E}(-,\tau) \tag{2b}$$

where

$$\mathrm{E}(+,\tau) = \exp[-(\lambda+\eta)\tau] \quad \text{and} \quad \mathrm{E}(-,\tau) = \exp[-(\lambda-\eta)\tau]$$

The components of the proton doublet, $\mathbf{I}_+^\alpha$ and $\mathbf{I}_+^\beta$, can be written as follows:

$$\mathbf{I}_+^\alpha = \mathbf{I}_+\left(\frac{1}{2} + \mathbf{S}_z\right) \tag{3a}$$

$$\mathbf{I}_+^\beta = \mathbf{I}_+\left(\frac{1}{2} - \mathbf{S}_z\right) \tag{3b}$$

By combining eqs 2 and 3, the following expression for the evolution of proton transverse magnetization after time τ is obtained:

$$\sigma(\tau) = \mathbf{I}_+^\alpha(\tau) + \mathbf{I}_+^\beta(\tau) = \mathbf{I}_+^\alpha(0)\,\mathrm{E}(+,\tau) + \mathbf{I}_+^\beta(0)\,\mathrm{E}(-,\tau)$$

$$= \frac{\mathbf{I}_+}{2}[\mathrm{E}(+,\tau) + \mathrm{E}(-,\tau)] + \mathrm{I}_+\mathbf{S}_z[\mathrm{E}(+,\tau) - \mathrm{E}(-,\tau)] \tag{4}$$

Equation 4 shows that, as a result of the differential relaxation rate between the two proton components, after time τ the in-phase proton magnetization has been partially converted into antiphase magnetization with respect to nitrogen.

Assuming axial symmetry for the CSA interaction, the expressions for the auto relaxation rate, λ, and the cross-correlation rate, η, are[11,13,14]

$$\lambda = D[4J^{dd}(0) + 4\alpha^2 J^{cc}(0) + 3\alpha^2 J^{cc}(\omega_H) + 3J^{dd}(\omega_H) + 3J^{dd}(\omega_H - \omega_N) + 3J^{dd}(\omega_N) + 6J^{dd}(\omega_H + \omega_N)] \tag{5}$$

and

$$\eta = 2\alpha D[4J^{cd}(0) + 3J^{cd}(\omega_H)] \tag{6}$$

with:

(19) Dalvit, C. *J. Magn. Reson.* **1991**, *95*, 410−416.
(20) Tjandra, N.; Szabo, A.; Bax, A. *J. Am. Chem. Soc.* **1996**, *118*, 6986−6991.
(21) Vis, H.; Boelens, R.; Mariani, M.; Stroop, R.; Vorgias, C. E.; Wilson, K. S.; Kaptein, R. *Biochemistry* **1994**, *33*, 14858−14870.
(22) Vis, H.; Mariani, M.; Vorgias, C. E.; Wilson, K. S.; Kaptein, R.; Boelens, R. *J. Mol. Biol.* **1995**, *254*, 692−703.
(23) Vis, H.; Vorgias, C. E.; Wilson, K. S.; Kaptein, R.; Boelens, R. *J. Biol. NMR* In press.
(24) Delaglio, F.; Grzesiek, S.; Vuister, G. W.; Zhu, G.; Pfeifer, J.; Bax, A. *J. Biol. NMR* **1995**, *6*, 277−293.

$$D = \frac{1}{8}\left(\frac{\mu_0}{4\pi}\right)^2(\gamma_N\gamma_H\hbar r_{NH}^{-3})^2 \quad (7)$$

$$\alpha = -\frac{2}{3}\left(\frac{4\pi}{\mu_0}\right)B_0(\sigma_{||} - \sigma_\perp)r_{NH}^{3}/(\hbar\gamma_N) \quad (8)$$

where α is defined as the ratio of the strength of CSA and dipolar interactions, r_{NH} denotes the $^1H_N-^{15}N$ internuclear distance, taken to be 1.02 Å, $\sigma_{||}$ and $\sigma_\perp$ denote the parallel component, aligned with the unique axis, and perpendicular component of the chemical shielding tensor, respectively, and $J^{dd}(\omega)$, $J^{cc}(\omega)$, and $J^{cd}(\omega)$ are the spectral density functions for dipolar autocorrelation, CSA autocorrelation, and dipolar-CSA cross correlation:

$$J^{pq}(\omega) = {}^2/_5\int_0^\infty \langle Y_{2,0}(\Omega^p(0))Y_{2,0}(\Omega^q(\tau))\rangle \cos(\omega\tau)\, d\tau \quad (9)$$

where $\Omega^p(t)$ describes the orientation of the principal axes of the interaction p at time t in the lab frame. For a rigid molecule with isotropic rotational diffusion the following relations between the spectral density functions hold:[11]

$$J(\omega) = J^{dd}(\omega) = J^{cc}(\omega) = J^{cd}(\omega)/\left(\frac{3\cos^2(\theta) - 1}{2}\right) \quad (10)$$

where θ is the angle between the axis of the CSA and dipolar tensors. As was pointed out by Tjandra et al.,[20] in the presence of internal motion that can be described by equivalent independent restricted rotations around three mutually orthogonal axes, this relation is still a very good approximation provided the angle θ is small. In this case eq 6 becomes:

$$\eta = 2\alpha D[4J(0) + 3J(\omega_H)]\left(\frac{3\cos^2(\theta) - 1}{2}\right) \quad (11)$$

which reduces to

$$\eta \approx 8\alpha D\, J(0)\left(\frac{3\cos^2(\theta) - 1}{2}\right) \quad (12)$$

for biological macromolecules since $J(\omega_H)$ is about two orders of magnitude smaller than $J(0)$.[25,26]

Measurement of Cross Correlation

The pulse sequence used for the quantitative measurement of $CSA(^1H_N)/DD(^1H_N-^{15}N)$ consists of an HSQC-type experiment in which the INEPT step has been replaced by a period of constant duration $4T$, which serves different purposes in two variations of the sequence. In the first variation (scheme A), the magnetization terms originating from the cross correlation between $CSA(^1H_N)$ and $DD(^1H_N-^{15}N)$ are selected. In the second variation (scheme B), the magnetization terms subjected to autorelaxation in the absence of interference effects are selected. The magnetization selected in both schemes experiences an identical number of pulses and lengths of the delays, so that no additional loss of signal other than relaxation needs to be considered. It should also be noted that both schemes have an identical dephasing resulting from passive homonuclear couplings.

In the pulse sequence corresponding to scheme A the evolution of proton magnetization due to chemical shift and heteronuclear $^1J_{NH_N}$ scalar coupling is refocused at the end of the $4T$ period, while the cross-correlation $CSA(^1H_N)/DD(^1H_N-^{15}N)$ is active for a time 4Δ. Palmer et al.[27] have shown that the application of a ^1H 180° pulse in the middle of an evolution period of length τ can suppress the antiphase magnetization arising from $CSA(^{15}N)/DD(^1H_N-^{15}N)$ cross correlation up to the second order in τ, whereas it is greatly reduced for higher orders. In analogy, the suppression of the terms arising from $CSA(^1H_N)/DD(^1H_N-^{15}N)$ cross correlation during the time $4(T - \Delta)$ is accomplished with the ^{15}N 180°(ϕ_6) and ^{15}N 180°(ϕ_7) pulses.

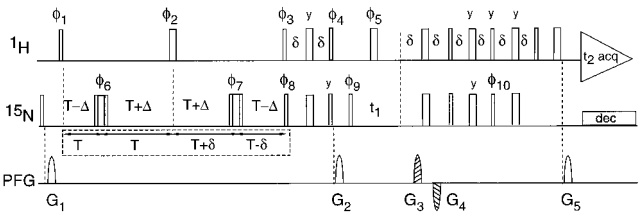

Figure 1. Pulse scheme for the quantitative measurement of cross correlation between ^1H_N CSA and $^1H_N-^{15}N$ dipolar interaction. Narrow and wide pulses correspond to flip angles of 90° and 180°, respectively. Scheme A is used to record the magnetization terms arising from CSA(^1H_N)/DD($^1H_N-^{15}N$) cross correlation in the period 4Δ. The gray-colored pulse is only applied in scheme B (*see below*). In the reference experiment (scheme B), the ^{15}N composite 180°(ϕ_6) and 180°(ϕ_7) pulses are applied at time T and $4T$ - δ (boxed), respectively, in order to select the antiphase magnetization generated by the heteronuclear $^1J_{NH_N}$ scalar coupling. In addition, the gray-colored ^1H 90°(ϕ_4) pulse is applied in order to move the water magnetization back to the z axis.[30] The phase of all pulses is assumed x, unless indicated. Delay durations: $T = 5.125$ ms; $\delta = 2.7$ ms; $4\Delta = 4$, 8, 12, 16, 20 ms. Phase cycling: $\phi_1 = 2(-x), 2x$; $\phi_2 = y, -y, x, -x$; $\phi_3 = x$ (scheme A) or $\phi_3 = y, -y$ (scheme B); $\phi_4 = 2(-x), 2x$ (scheme B only); $\phi_5 = 16x, 16(-x)$; $\phi_6 = 16x, 16(-x)$;); $\phi_7 = 32x, 32(-x)$; $\phi_8 = 4x, 4(-x)$; $\phi_9 = 8x, 8(-x)$; $\phi_{10} = y$; receiver $= 4x, 4(-x), 4(-x), 4x$ (scheme A) or receiver $= 2(x,-x), 4(-x,x), 2(x,-x)$ (scheme B). Quadrature detection in the t_1 dimension is accomplished by PFG coherence selection, in combination with a sensitivity enhancement scheme.[29] $G_{1,2,3,4,5} = 2$ ms, 15 G/cm; 1 ms, 20 G/cm; 2 ms, −20 G/cm; 2 ms, 20 G/cm; 1 ms, 8.112 G/cm.

The evolution of the relevant components of proton magnetization during the period $4T$ is described in the following, using the product operator formalism,[28] including only heteronuclear scalar coupling (J), autorelaxation (λ), and cross-relaxation processes (η). Again, proton and nitrogen angular momentum operators are denoted as **I** and **S**, respectively.

$$\mathbf{I}_z \xrightarrow{90°_{\phi_1}(\mathbf{I})} \mathbf{I}_y \xrightarrow{\lambda} \mathbf{I}_y \exp[-4\lambda(T - \Delta)] \xrightarrow{\eta}$$

$$\mathbf{I}_y\,\mathbf{S}_z \exp[-4\lambda(T - \Delta)][E(+,4\Delta) - E(-,4\Delta)] + \frac{\mathbf{I}_y}{2}\exp[-4\lambda(T - \Delta)][E(+,4\Delta) + E(-,4\Delta)] \quad (13)$$

The antiphase component originating from the $CSA(^1H_N)/DD(^1H_N-^{15}N)$ cross terms is transferred to ^{15}N by the ^1H 90°(ϕ_3) and ^{15}N 90°(ϕ_8) pulses and refocused *via* the heteronuclear $^1J_{NH_N}$ scalar coupling during the following period of duration 2δ. Before applying the purging gradient, G_3, the in-phase ^{15}N magnetization is transferred into z magnetization. The undesired in-phase proton magnetization, $\mathbf{I}_y$, which greatly exceeds the antiphase component at the end of the $4T$ period, is transferred into z magnetization by the proton 90°(ϕ_3) pulse. Subsequently, after the period 2δ, the proton magnetization is moved back to the xy plane and dephased by the purging gradient G_3. This scheme has proven to effectively suppress all the undesired

(25) Peng, J. W.; Wagner, G. *J. Magn. Reson.* **1992**, *98*, 308−650.
(26) Habazettl, J.; Wagner, G. *J. Magn. Reson. B* **1995**, *95*, 100−104.
(27) Palmer, A. G., III; Skelton, N. J.; Chazin, W. J.; Wright, P. E.; Rance, M. *Mol. Phys.* **1992**, *75*, 699−711.
(28) Sørensen, O. W.; Eich, G. W.; Levitt, M. H.; Bodenhausen, G.; Ernst, R. R. *Prog. NMR Spectrosc.* **1983**, *16*, 163−192.

components of proton magnetization. After the purging gradient, the ^{15}N magnetization is moved to the *xy* plane for chemical shift labeling during t_1 and transferred back to the proton for detection by a reverse-INEPT with pulsed-field gradient sensitivity enhancement.[29]

According to eq 13 the signal intensity measured with scheme A is

$$I^{cd} = \frac{C}{2}\exp[-4\lambda(T-\Delta)][E(+,4\Delta) - E(-,4\Delta)]\cos\xi \quad (14)$$

where C is a proportionality factor resulting from experimental setup and $\cos\xi = \cos(4\pi J_{H^NH^\alpha}T)$ accounts for the dephasing resulting from the evolution of the $^3J_{H^NH^\alpha}$ homonuclear scalar coupling during $4T$.

Scheme B of the pulse sequence is used to record the reference spectrum, *i.e.* the in-phase component in the absence of interference effects during the $4T$ period. During the time 2δ the cross correlation is active, but its effect on the measured intensity of signal can be safely neglected (*vide infra* eq 17). Again, describing the evolution of the relevant components of proton magnetization in terms of product operators:

$$\mathbf{I}_z \xrightarrow{90°_{\phi_1}(\mathbf{I})} \mathbf{I}_y \xrightarrow{\lambda} \mathbf{I}_y\exp[-\lambda(4T-2\delta)] \xrightarrow{\eta}$$

$$\mathbf{I}_y\mathbf{S}_z\exp[-\lambda(4T-2\delta)][E(+,2\delta) - E(-,2\delta)] + \frac{\mathbf{I}_y}{2}\exp[-\lambda(4T-2\delta)][E(+2\delta) + E(-,2\delta)] \quad (15)$$

The heteronuclear $^1J_{NH_N}$ scalar coupling is active for a time 2δ during the period $4T$, so that proton in-phase magnetization evolves to antiphase with respect to nitrogen and *vice versa*:

$$\xrightarrow{J} -\frac{\mathbf{I}_x}{2}\exp[-\lambda(4T-2\delta)][E(+,2\delta) - E(-2\delta)] \times \sin(2\pi^1 J_{NH_N}\delta)$$

$$-\mathbf{I}_y\mathbf{S}_z\exp[-\lambda(4T-2\delta)][E(+,2\delta) + E(-,2\delta)] \times \sin(2\pi^1 J_{NH_N}\delta) \quad (16)$$

For $\delta = 2.7$ ms the factor $\sin(2\pi^1 J_{NH_N}\delta)$ can safely be equated to one since small differences in the value of the $^1J_{NH_N}$ coupling constant in the range 90−100 Hz introduce a negligible systematic error (less than 1%) in the measured intensity of the signal.

The proton antiphase magnetization, $\mathbf{I}_x\mathbf{S}_z$, is transferred to ^{15}N by the ^1H 90°(ϕ_3) pulse, shifted in phase now by 90° with respect to scheme A, and the ^{15}N 90°(ϕ_8) pulse, and subsequently refocused to in-phase ^{15}N magnetization during the following period 2δ. Again, before applying the purging gradient G_3, the ^{15}N magnetization is transferred into *z* magnetization. The unwanted proton in-phase component is removed in the same way as in scheme A. The additional proton pulse placed before the gradient brings the water magnetization along the *z* axis, according to the water-flip-back scheme.[30] The remainder of the pulse sequence is exactly the same as in scheme A.

According to eq 16, the signal intensity of the reference spectrum measured with scheme B is given by the following expression:

(29) Kay, L. E.; Keifer, P.; Saarinen, T. *J. Am. Chem. Soc.* **1992**, *114*, 10663−10665.

(30) Grzesiek, S.; Bax, A. *J. Am. Chem. Soc.* **1993**, *115*, 12593−12594.

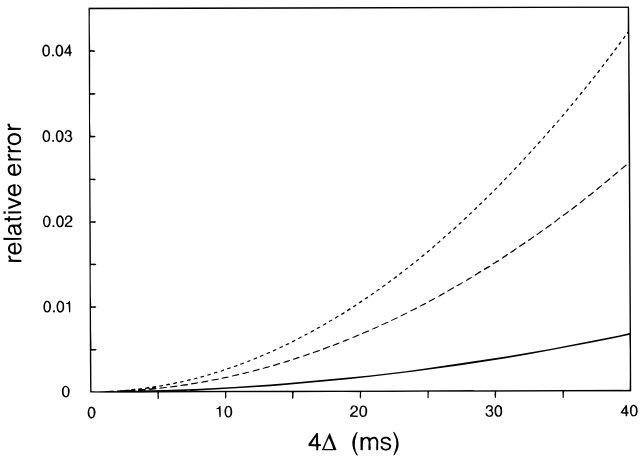

Figure 2. Plots of the relative error introduced by the linear approximation (cf. eq 18) as a function of the period 4Δ, assuming $4T = 40$ ms, $\lambda = 50$ s^{-1}, and $\eta = 5$ (solid line), 10 (dashed line), and 12.5 s^{-1} (dotted line).

$$I^{ref} = \frac{C}{2}\exp[-\lambda(4T-2\delta)][E(+,2\delta) + E(-,2\delta)]\cos\xi$$
$$= C\exp(-4\lambda T)\exp(-2\eta\delta)\cos\xi$$
$$\approx C\exp(-4\lambda T)\cos\xi \quad (17)$$

The approximation in eq 17 holds to a very good extent: the error introduced for $2\delta = 5.4$ ms and η in the range 1−10 s^{-1} is in the order of 10^{-3} %.

The ratio of the signal intensities obtained with the two schemes, using eqs 14 and 17, is

$$\frac{I^{cd}}{I^{ref}} = \frac{\exp(4\lambda\Delta)}{2}[E(+,4\Delta) - E(-,4\Delta)] \approx -4\eta\Delta \quad (18)$$

The relative error introduced by the linear approximation in eq 18 is shown in Figure 2 as a function of the period 4Δ, for different values of the ratio η/λ, assuming $4T = 40$ ms and $\lambda = 50$ s^{-1}. Clearly, the assumption of a linear buildup of the intensity ratio is a very good approximation even for values of 4Δ that largely exceed the proton autorelaxation time $1/\lambda$ assuming an unrealistically large ratio $\eta/\lambda = 0.25$.

A buildup curve of the ratio I^{cd}/I^{ref} can be obtained by recording several 2D experiments at different values of Δ, while keeping the other experimental parameters constant. Only one reference is required for a buildup series. A linear fit of the buildup curve will provide the value of the cross-correlation rate η. Alternatively, two 2D experiments can be acquired corresponding to a single point of the curve. In this case, the cross-correlation rate is derived by direct application of eq 18.

Results and Discussion

The experiment for measuring the CSA(^1H_N)/DD(^1H_N−^{15}N) cross-correlation rate was performed on a solution of 1 mM uniformly ^{15}N labeled HUBst in 90% ^1H_2O/10% ^2H_2O as described in the Experimental Section. The buildup of the antiphase term originating from cross-correlation effects can be monitored by varying the duration of the parameter Δ (cf. Figure 1). Setting $\Delta = 0$ provides a simple method for checking the quality of the experiment, as no buildup can occur and no signal should be detected. An experiment on the HUBst sample, performed with $\Delta = 0$ and with an identical experiment time as used on the other data, displays only thermal noise in the resulting spectrum (data not shown), indicating that all detected signal for values $\Delta > 0$ originates from the CSA/DD pathway.

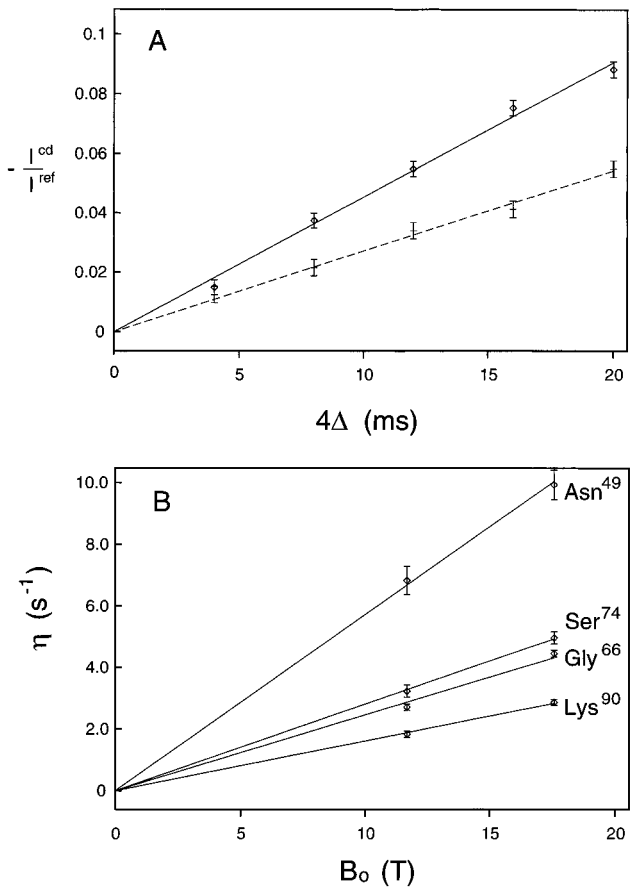

Figure 3. (A) Buildups of the $-I^{cd}/I^{ref}$ ratio for residue Gly-66 at 11.7 T (dashed) and 17.6 T solid line). The curves obtained from least-squares linear fits of the intensity ratio $-I^{cd}/I^{ref}$ *vs* the time interval 4Δ, using eq 18, are shown. (B) Least-squares linear fit of η *vs* the static field B_0 for four different residue in HUBst.

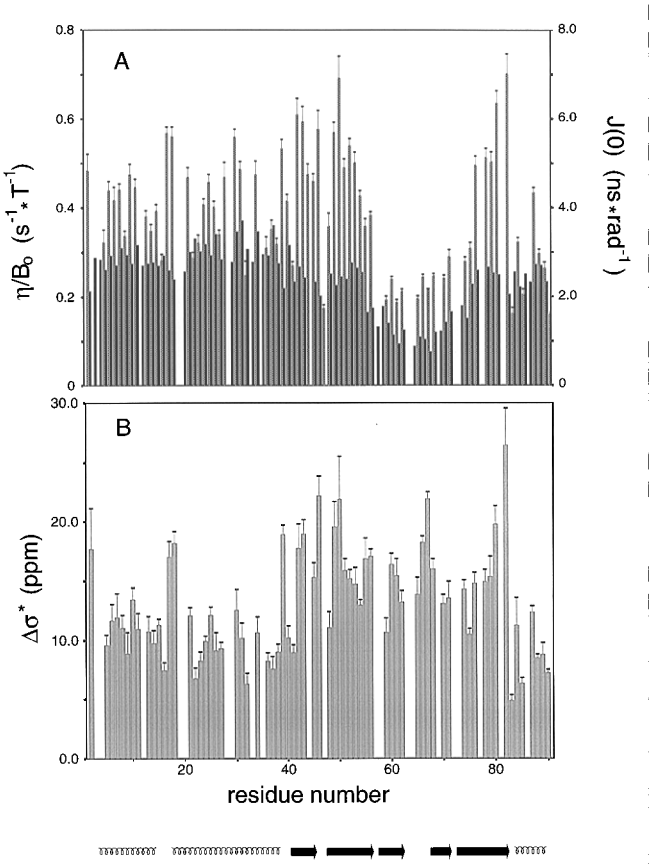

Figure 4. (A) Bar graphs of the ratio η/B_0 (grey) and the spectral density at zero frequency, J(0) (black), as a function of residue number in HUBst. (B) Bar graphs of $\Delta\sigma^*$ (which equals $(\sigma_{\parallel} - \sigma_{\perp})(3\cos^2(\theta) - 1)/2$) as a function of the residue number in HUBst. Secondary structure elements, as identified in HUBst,[21,22] are indicated.

In Figure 3A the buildup curve of the ratio $-I^{cd}/I^{ref}$ is shown for residue Gly-66 at 11.6 and 17.6 T as a function of time 4Δ during which the CSA/DD interference is active. As the peaks in the CSA/DD spectrum are of opposite sign as compared to the peaks in the reference spectrum, the cross-correlation rate is positive. This is in agreement with the results obtained from a ^{15}N HSQC experiment on HU in which the amide protons were not decoupled from ^{15}N during acquisition (data not shown). In this spectrum, the high-field shifted multiplet component has the larger intensity, also implying a positive η (cf. eq 1).

In agreement with eq 18 the measured points for Gly-66 are well fitted by a straight line passing through the origin. The correlation of dipolar interactions involving *different* proton pairs could in principle interfere with the measurement of the CSA(^{1}H$_N$)/DD(^{1}H$_N-^{15}$N) cross-correlation rate, both by affecting the buildup of the desired $\mathbf{I}_y\mathbf{S}_z$ and by attenuating the intensity of the reference experiment. To estimate the possible effects of these processes the CSA(^{1}H$_N$)/DD(^{1}H$_N-^1$H$_i$) and DD(^{1}H$_N-^1$H$_i$)/DD(^{1}H$_N-^1$H$_j$) cross-correlation rates involving other proton spins, ^{1}H$_i$ and ^{1}H$_j$, were calculated on the basis of the average NMR structure of HUBst for each amide proton by assuming a rigid isotropically tumbling molecule with a correlation time τ_c = 9 ns. On average, it was found that these rates are 2−3 s^{-1}, which is a factor 2−5 slower than the measured CSA(^{1}H$_N$)/DD(^{1}H$_N-^{15}$N) rates. The time dependence of the density matrix for a spin system consisting of 3 proton spins in addition to the ^{1}H$_N-^{15}$N spins was then numerically solved. This simulation of the experiment showed that the CSA(^{1}H$_N$)/DD(^{1}H$_N-^1$H$_i$) and DD(^{1}H$_N-^1$H$_i$)/DD(^{1}H$_N-^1$H$_j$) processes only marginally affect the measurements of the CSA(^{1}H$_N$)/DD(^{1}H$_N-^{15}$N) rate, introducing a systematic underestimate of 1−2% well below the experimental error.

The difference in the slope measured at 11.6 and 17.6 T (cf. Figure 3B) reflects the dependence of the cross-correlation rate η on the static field B_0. Equation 11 shows that the values of η are also dependent upon the motional behavior of the ^{1}H$_N-^{15}$N bond vector. The values of J(0) and J(ω_H) at 11.6 and 17.6 T were determined previously by using a reduced spectral density mapping procedure from experimental ^{15}N relaxation data of HUBst.[23] By using these values, it can be calculated that the approximation made to derive eq 12 introduces an error less than 1% for the residues in the core and ca. 1−2% for the residues in the most flexible regions. Thus, the assumption of a linear dependence of the cross-correlation rate η on the static field B_0, in agreement with eq 12, is expected to introduce a negligible error. This is illustrated in Figure 3B where the linear fits of the values of η measured at 11.6 and 17.6 T *vs* the static field B_0 are shown for the residues Asn-49, Gly-66, Ser-74, and Lys-90. Different values of the slope η/B_0 are observed, resulting from differences in local mobility and/or in the chemical shielding tensor (cf. eq 12).

The measured values of η/B_0 for HUBst, as a function of residue number, are shown in Figure 4A. They span a range of 0.16−0.70 s^{-1} T^{-1}, which largely exceeds the average error of 0.02 s^{-1} T^{-1}. The values of the spectral density at zero frequency, J(0), for HUBst are also shown in Figure 4A as a function of residue number. As expected, residues 55−75 in the highly mobile β-arms[23] of HUBst show values of η/B_0 lower than those of the remainder of the protein.

By using the values of J(0), the measured η/B_0 values can be corrected for the dynamic properties of the $^1H_N-^{15}N$ bond vector with eq 12, provided that the underlying assumptions for deriving eq 11 are fullfilled. For almost all residues in the core the dynamics of the backbone NH vectors is satisfactorily described by an overall isotropic tumbling with correlation time of 8.9 ns, with superimposed internal fast motion (correlation times in the 1−20 ps range) as described by a conventional Lipari-Szabo model. For some residues in the β-arms, improvements were obtained by using an extended model, including an additional slower motion. However, no statistically significant improvements were obtained by using an anisotropic tumbling model.[23]

The values of $\Delta\sigma^*$, which equals $(\sigma_{||} - \sigma_\perp)(3\cos^2(\theta) - 1)/2$, were calculated with eqs 7, 8, and 12, and are shown in Figure 4B as a function of residue number in HUBst. Since the measured cross-correlation rates are all positive, all $\Delta\sigma^*$ values are positive. However, both an axially symmetric tensor with the unique component aligned along the NH-bond vector and $(\sigma_{||} - \sigma_\perp) > 0$, as well as an axially symmetric tensor with the unique component at an angle $\theta > 54.4°$ with respect to the NH bond vector and $(\sigma_{||} - \sigma_\perp) < 0$, would result in positive values of $\Delta\sigma^*$. In the presence of internal motions, the latter condition would violate the underlying assumptions of our analysis.

The values measured for HUBst span a range of 5−26 ppm with an average experimental error of 1 ppm. The average value of $\Delta\sigma^*$ (13 ± 5 ppm) is in good agreement with the results of solid-state NMR measurement on *N*-acetyl-D,L-valine,[5] which showed an almost axially symmetric tensor with the unique component aligned along the NH bond vector. As was pointed out, the value of 13 ppm is intermediate between the shielding anisotropy of protons bound to carbon and protons involved in O−H···O bridges and is consistent with the fact that the amide protons are involved in rather weak hydrogen bonds.

Local conformation as well as hydrogen bonding are expected to vary both the magnitude and the orientation of the tensor components.[4,5,33] The dispersion of the values of $\Delta\sigma^*$ observed in Figure 4B also suggests a conformational dependency, but differences in the magnitude of the chemical shielding anisotropy or variations in the angle θ between the NH bond and the unique component of the chemical shielding tensor could both account for the observed variability.

The secondary structure elements identified in HUBst[21,22] are also depicted in Figure 4. It is apparent that, on average, the residues in α-helical conformation have a lower value of $\Delta\sigma^*$ than those in β-sheet regions, the differences being much larger than the experimental error. On the basis of the ensemble of 25 NMR structures,[22] a detailed analysis of the hydrogen bond geometry for the backbone amide protons of HUBst has been carried out with the MOLMOL package,[31] in order to select the residues for which the distance between the nitrogen donor and the carbonyl acceptor was not larger than 3.7 Å and the ∠ONH angle was less than 35°. The histograms of $\Delta\sigma^*$ for the selected residues, considering only those in regular α-helix and β-sheet regions and displaying a proper hydrogen bond as described above, are shown in Figure 5. The residues in α-helical conformation show a rather small dispersion (4 ppm) around the average value of $\Delta\sigma^*_{helix}$ (ca. 8−9 ppm). It is worth noting that the first two residues of the second helix, Ser-17 and Lys-18, show very large deviations (ca. 9 ppm) with respect to the average value of $\Delta\sigma^*_{helix}$ (cf. Figure 4B). Although their backbone geometry is in α-helical conformation, they do not have a proper hydrogen-bonding geometry. It is for this reason that they have not been included in the histogram of Figure 5. The residues in β-sheet regions show a somewhat larger dispersion in the values of $\Delta\sigma^*$: the average value is located at ca. 16 ppm, and the observed range is 6 ppm. The average values of $\Delta\sigma^*$ for α-helix and β-sheet differ by ca. 6−7 ppm, and from the histograms in Figure 5 it appears that the overlap between the two distributions is small. Calculations have explained the well-known relationship between the isotropic chemical shift of the amide protons and the length of the hydrogen bond.[32] However, the differences observed between helices and sheets were explained by effects other than the direct effects of hydrogen bonding. The upfield shift upon helix formation, as compared to the downfield shift in β-sheets, was explained in terms of the effects originating on the residues $i - 2$ and $i - 3$.[32] Clearly, the $\Delta\sigma^*$ data show a similar pattern, being affected both by hydrogen bonding and by the presence of secondary structural elements.

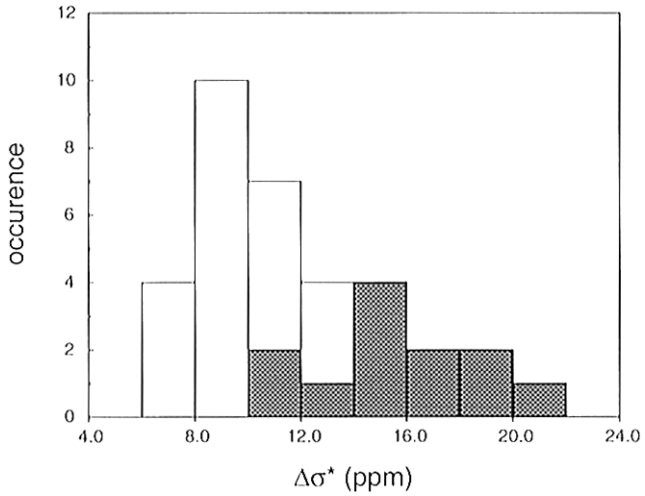

Figure 5. Histograms of the values $\Delta\sigma^*$ for the residues of HUBst in regular α-helix (empty) or β-sheet conformations (filled) displaying a proper hydrogen bond (see text).

Conclusions

The experiment presented allows the quantitative measurement of the ^1H_N CSA/$^1H_N-^{15}N$ dipolar cross-relaxation rate in ^{15}N-enriched proteins. The CSA parameter, $\Delta\sigma^*$, can be extracted from these rates provided that the motional behavior of the $^1H-^{15}N$ bond vector is known from ^{15}N relaxation studies. The data recorded for HUBst show a clear dependence of $\Delta\sigma^*$ upon hydrogen bond formation and secondary structure. To the best of our knowledge, these data present the first measurement of the ^1H_N CSA for a large fraction of the residues in a single protein, and thus provide the first insight of the dependence of the proton CSA upon secondary structure in biological macromolecules.

Acknowledgment. G.W.V. has been financially supported by the Royal Netherlands Academy of Arts and Sciences. The data were acquired at the SONNMR Large-Scale Facility in Utrecht.

JA970573K

(31) Koradi, R.; Billeter, M.; Wüthrich, K. *J. Mol. Graphics* **1995**, *14*, 51−55.

(32) Asakura, T.; Taoka, K.; Demura, M.; Williamson, M. P. *J. Biomol. NMR* **1995**, *6*, 227−236.

(33) Chesnut, D. B.; Phung, C. G. *Chem. Phys. Lett.* **1991**, *183*, 505−509.